

Microbial dynamics in newly diagnosed and treatment naïve IBD patients in the Mediterranean

Authors: Rausch, Dr. Philipp^{1,2*}; Ellul, Dr. Sarah^{3*}; Pisani, Dr. Anthea⁴; Bang, Dr. Corinna¹; Tabone, Dr. Trevor⁴; Marantidis, Dr. Cordina Claire⁵; Zahra, Dr. Graziella⁶; Franke, Prof. Dr. Andre^{1#} & Ellul, Dr. Pierre^{4#}

¹ Institute of Clinical Molecular Biology, Christian-Albrechts-University of Kiel, Kiel, Germany

² Laboratory of Genomics and Molecular Biomedicine, Department of Biology, University of Copenhagen, Copenhagen, Denmark

³ Division of Pediatric Surgery, Department of Surgery, Mater Dei Hospital, Malta,

⁴ Division of Gastroenterology, Department of Medicine, Mater Dei Hospital, Malta

⁵ Department of Microbiology, Mater Dei Hospital, Malta

⁶ Molecular Diagnostics, Department of Pathology, Mater Dei Hospital, Malta

* equal contribution of PR and SE (joint first authors)

corresponding authors: Pierre Ellul (pierre.ellul@gov.mt), Andre Franke (franke@mucosa.de)

Supplemental materials and methods

DNA Extraction: DNA was extracted using the QIAamp DNA fast stool mini kit automated on the QIAcube (Qiagen, Hilden, Germany). Material is transferred to 0.70 mm Garnet Bead tubes (Dianova, Hamburg, Germany) filled with 1.1 ml ASL lysis buffer. Bead beating is performed using the a SpeedMill PLUS (Analytik Jena, Jena, Germany) for 45 s at 50 Hz. Samples are then heated to 95°C for 5 min with subsequent continuation of the manufacturer's protocol. DNA binds specifically to the QIAamp silica-gel membrane while contaminants pass through. PCR inhibitors are removed by the combined action of a unique adsorption resin and an optimized buffer. The approximate amount of DNA is between 10-40 µg per sample.

Bacterial 16S rRNA Gene Sequencing: Variable regions V1-V2 of the 16S rRNA gene are amplified using the primer pair 27F-338R in a dual-barcoding approach according to Caporaso *et al.* 2012¹. DNA is diluted 1:10 prior PCR, and 3 µl of this dilution are finally used for amplification. PCR-products are verified using the electrophoresis in agarose gel. PCR products are normalized using the SequelPrep Normalization Plate Kit (Thermo Fischer Scientific, Waltham, MA, USA), pooled in an equimolar fashion and sequenced on the Illumina MiSeq v3 2×300 bp (Illumina Inc., San Diego, CA, USA). Demultiplexing after sequencing was based on 0 mismatches in the barcode sequences via *bcl2fastq*.

Quality control, classification, and binning of sequences: Data processing was performed using the *DADA2* version 1.10² workflow for big datasets (<https://benjjneb.github.io/dada2/bigdata.html>) resulting in abundance tables of **Amplicon Sequence Variants (ASVs)**. All sequencing runs were handled separately for error correction, read merging, and combined chimera detection. ASVs underwent taxonomic annotation using the naïve Bayesian classifier implemented in *DADA2* using the Ribosomal Database Project 16 release as a taxonomic classification database^{3,4}. ASV sequences were aligned via NAST-alignment to the SILVA core database and filtered for informative sites (constant gaps, constant bases) in *mothur*⁵⁻⁸. Phylogenetic tree construction on ASV alignment generated was carried out using *FastTree 2.1* using the CAT substitution model with Γ -correction and improved accuracy, employing more minimum evolution rounds for initial tree search [-spr 4], more exhaustive tree search [-mlacc 2], and a slower initial tree search [-slownni]⁹.

Statistical methods for microbiome analyses: Microbiome data was rarefied to 11800 reads/sample to ensure comparable and sufficient coverage across samples during analysis (average Good's coverage 99.88% ± 0.001 SD).

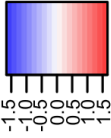
Alpha diversity: Phylogenetic measures of alpha diversity [Nearest Taxon Index (NTI), and Net Relatedness Index (NRI)] were derived using the *picante* package, based on 999 permutations against a null model preserving relative species richness within the communities^{10,11} [$NRI = -1 \times (MPD_{\text{observed}} - \text{mean}(MPD_{\text{random}})) / SD(MPD_{\text{random}})$; $NTI = -1 \times (MNTD_{\text{observed}} - \text{mean}(MNTD_{\text{random}})) / SD(MNTD_{\text{random}})$]. Both metrics are phylogenetic effect sizes, for which positive values indicate phylogenetic clustering, values close to zero indicate neutral or random community assembly, and negative values indicate phylogenetic overdispersion, either over the whole phylogenetic tree (NRI) or across the closest related species/tips of the phylogenetic tree (NTI).

Network analyses: To generate co-abundance networks we employed the *SparCC* algorithm as implemented in *mothur* (50 samplings, 100 iterations, 10,000 permutations, *P*-value adjustment via

Benjamini-Hochberg procedure) was used to generate co-abundance networks based on ASV abundances within the study cohorts (shared among 10% samples) at a P -value cutoff of $P_{FDR} \leq 0.05$ and a correlation strength above $|R| \geq 0.25$ ¹².

Supplemental figures

average Z-Value



■ Proteobacteria ■ Bacteroidetes ■ Firmicutes

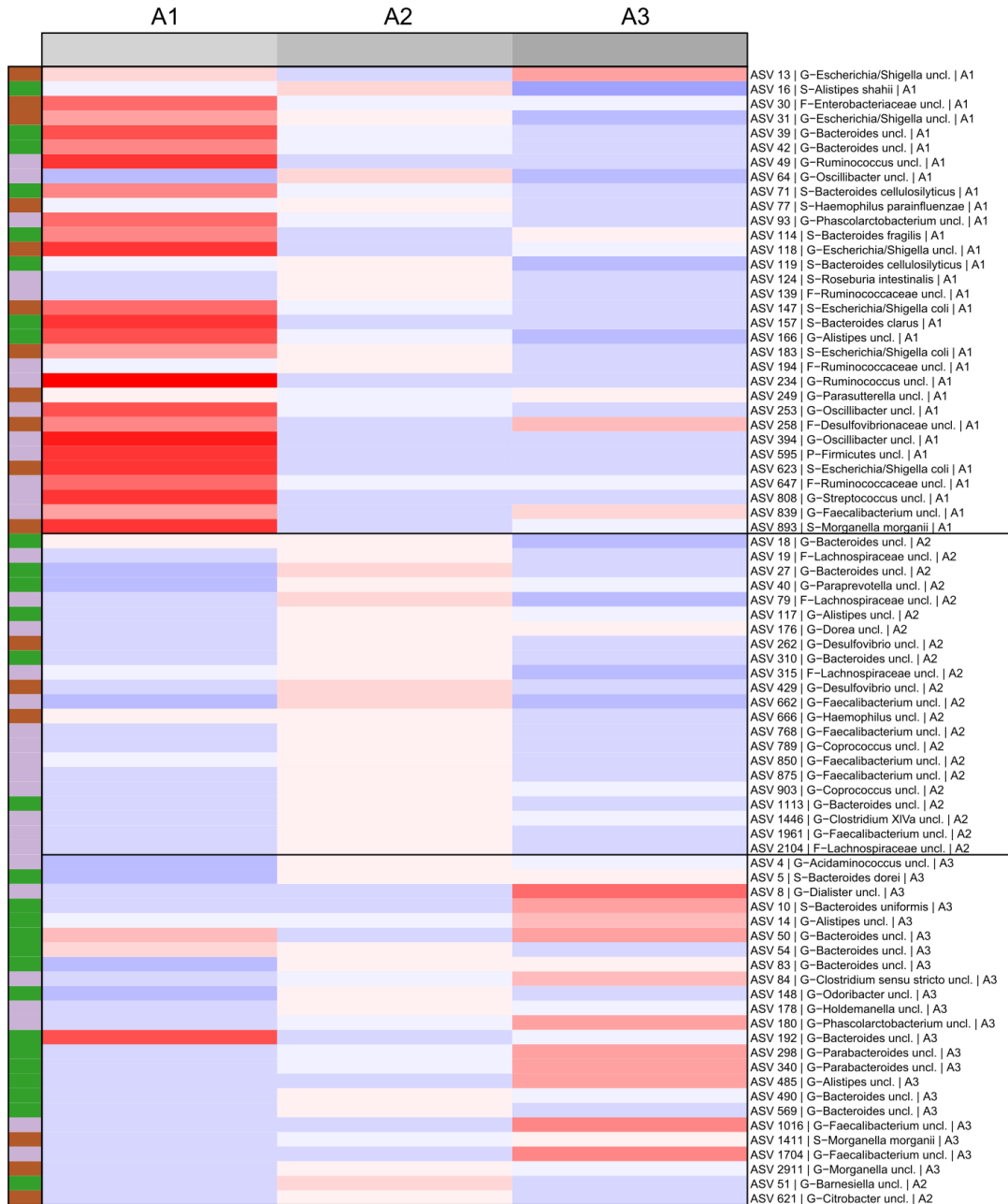
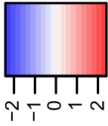


Figure S1: Heatmap visualizing significant differentially abundant ASVs in CD patients with respect to age subgroups following the Montreal classification (A1: <16 yrs., A2: 17-40 yrs., A3: >40 yrs., Table S3). Differential abundance was tested via *DESeq2* and only functions significant after p-value adjustment are displayed.

average Z-Value



Firmicutes
 Bacteroidetes
 Proteobacteria
 Actinobacteria

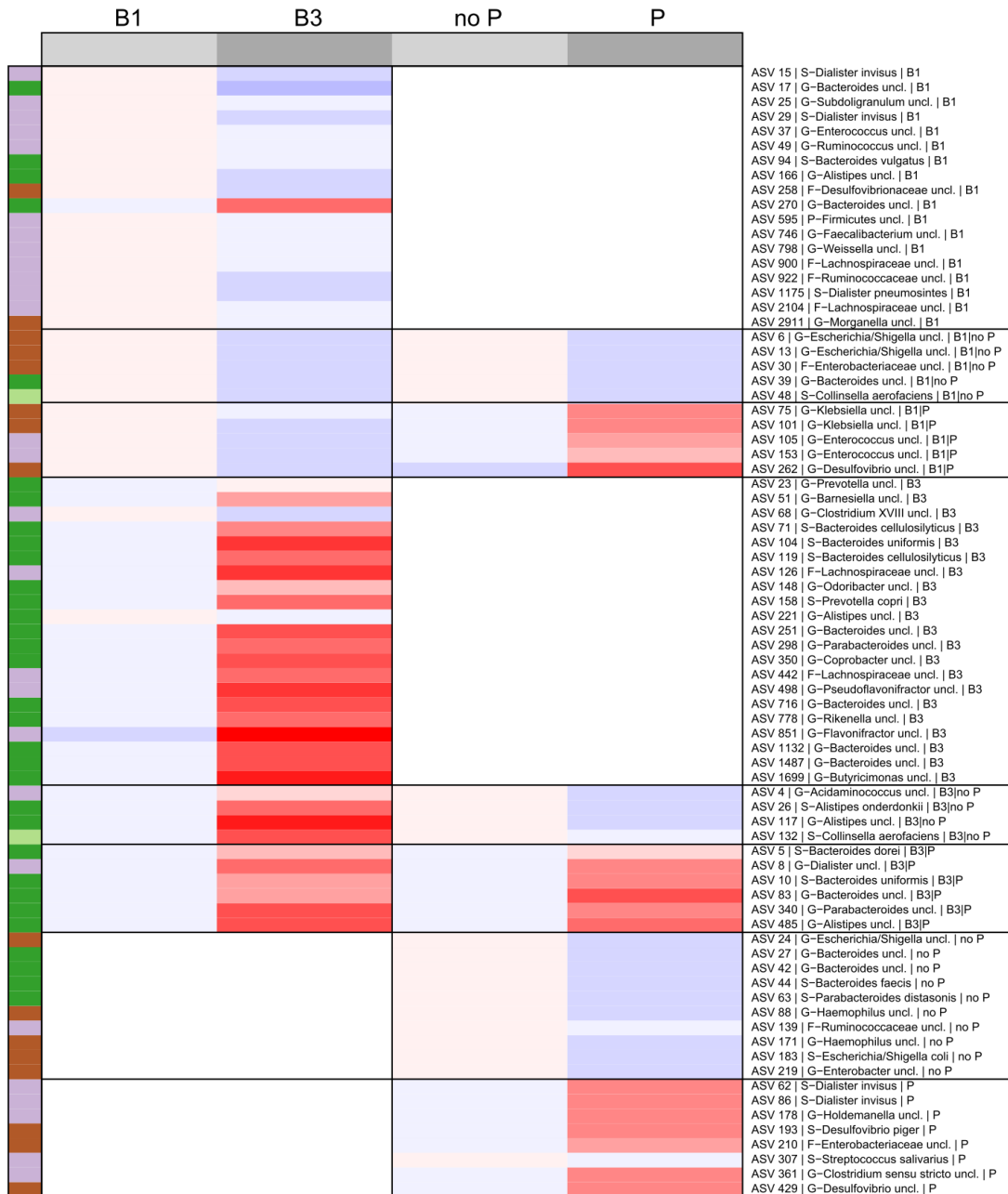
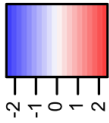


Figure S2: Heatmap visualizing significant differentially abundant ASVs in CD patients with respect to disease behavior subgroups following the Montreal classification (B1: non-stricturing/non-penetrating, B3: penetrating, Table S3), while using the classification of perianal disease as a separate subtype (P:

perianal disease manifestation, no-P: no perianal disease). Differential abundance was tested via DESeq2 and only functions significant after p-value adjustment are displayed.

average Z-Value



Firmicutes
 Actinobacteria
 Proteobacteria
 Bacteroidetes

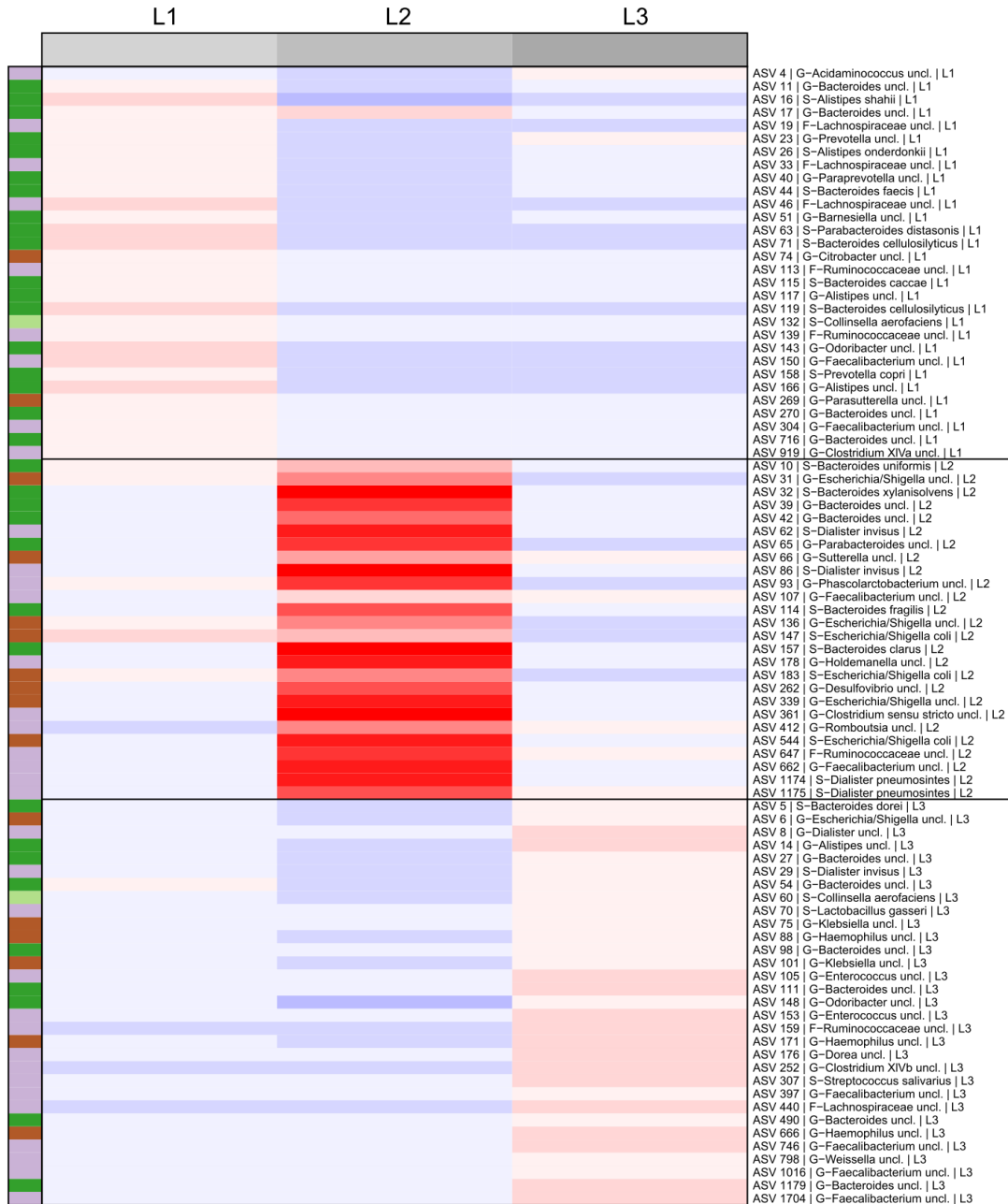
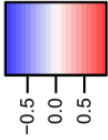


Figure S3: Heatmap visualizing significant differentially abundant ASVs in CD patients with respect to disease location subgroups following the Montreal classification (L1: ileal, L2: colonic, L3: ileocolonic, Table S3). Differential abundance was tested via DESeq2 and only functions significant after p-value adjustment are displayed.

average Z-Value



Firmicutes
 Actinobacteria
 Bacteroidetes

 Proteobacteria

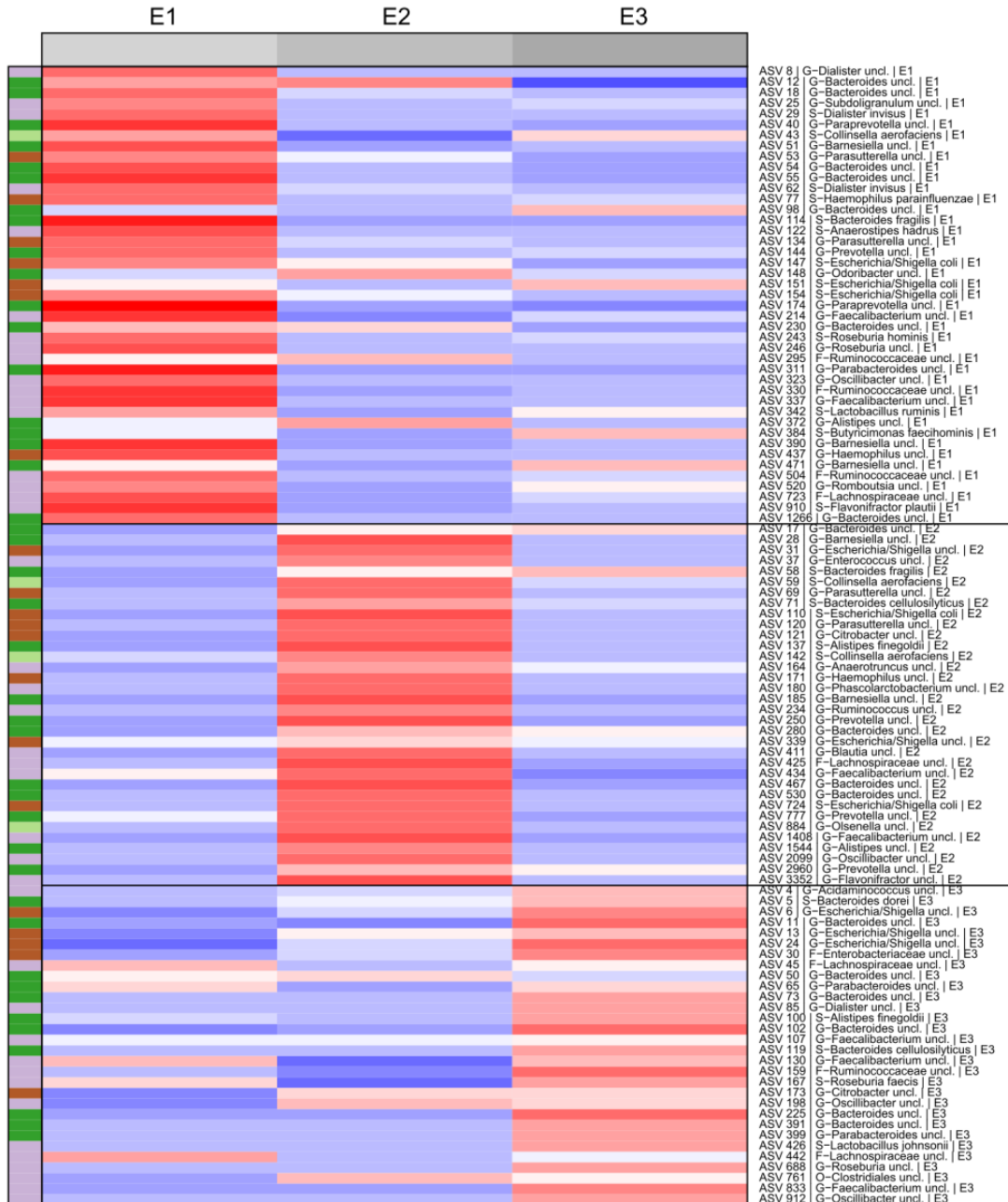
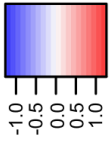


Figure S4: Heatmap visualizing significant differentially abundant ASVs in UC patients with respect to age subgroups following the Montreal classification (E1: Ulcerative proctitis, E2: left sided UC (distal UC), E3: extensive UC (pancolitis), Table S3). Differential abundance was tested via DESeq2 and only functions significant after p-value adjustment are displayed.

average Z-Value



■ Bacteroidetes
 ■ Firmicutes
 ■ Proteobacteria
■ Actinobacteria

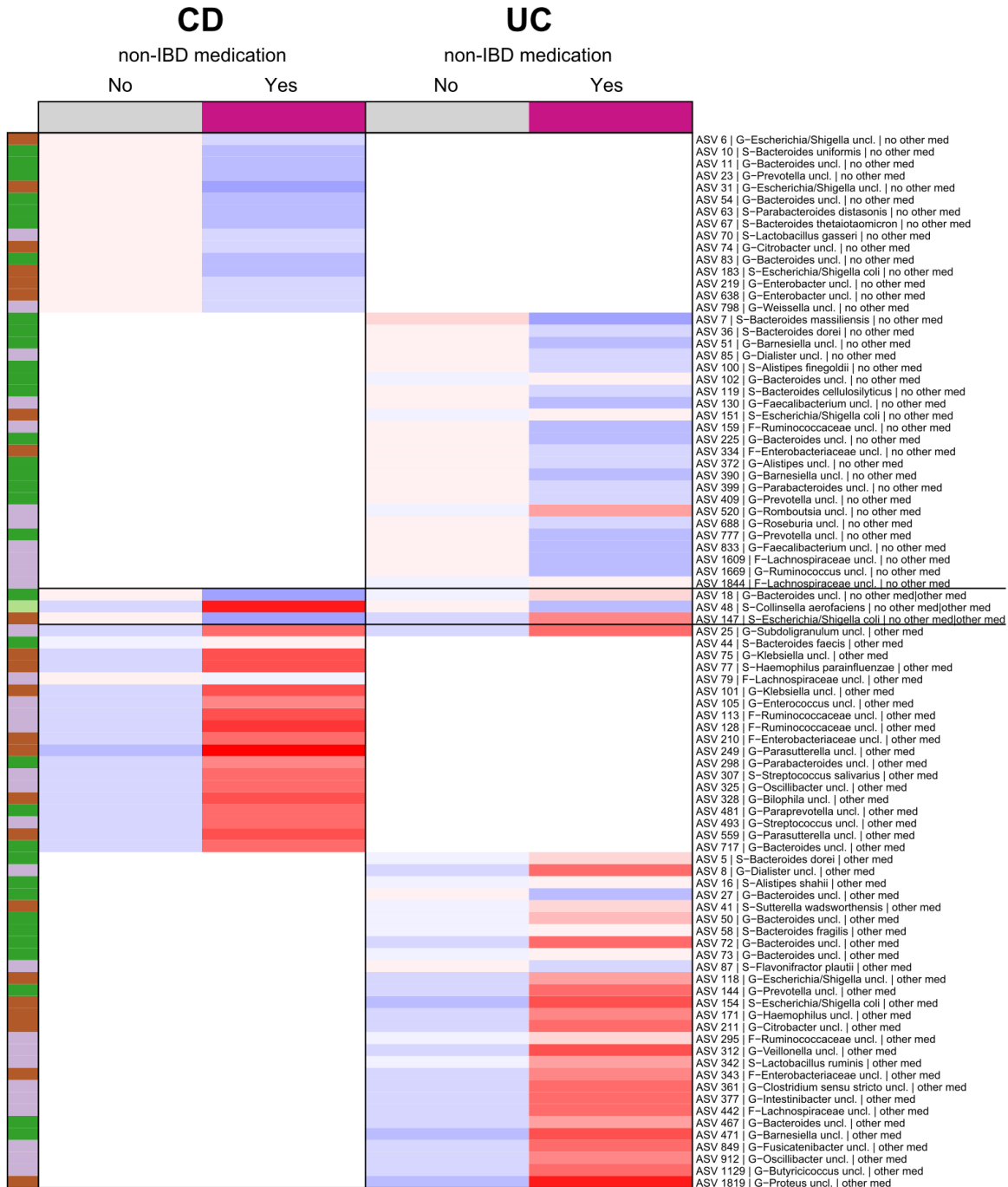
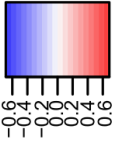


Figure S5: Heatmap visualizing significant differentially abundant ASVs in CD and UC patients with respect to prior antibiotic treatments (Table S5). Differential abundance was tested via DESeq2 and only functions significant after p-value adjustment are displayed.

average Z-Value



- Bacteroidetes
- Firmicutes
- uncl. Bacteria
- Actinobacteria
- Proteobacteria

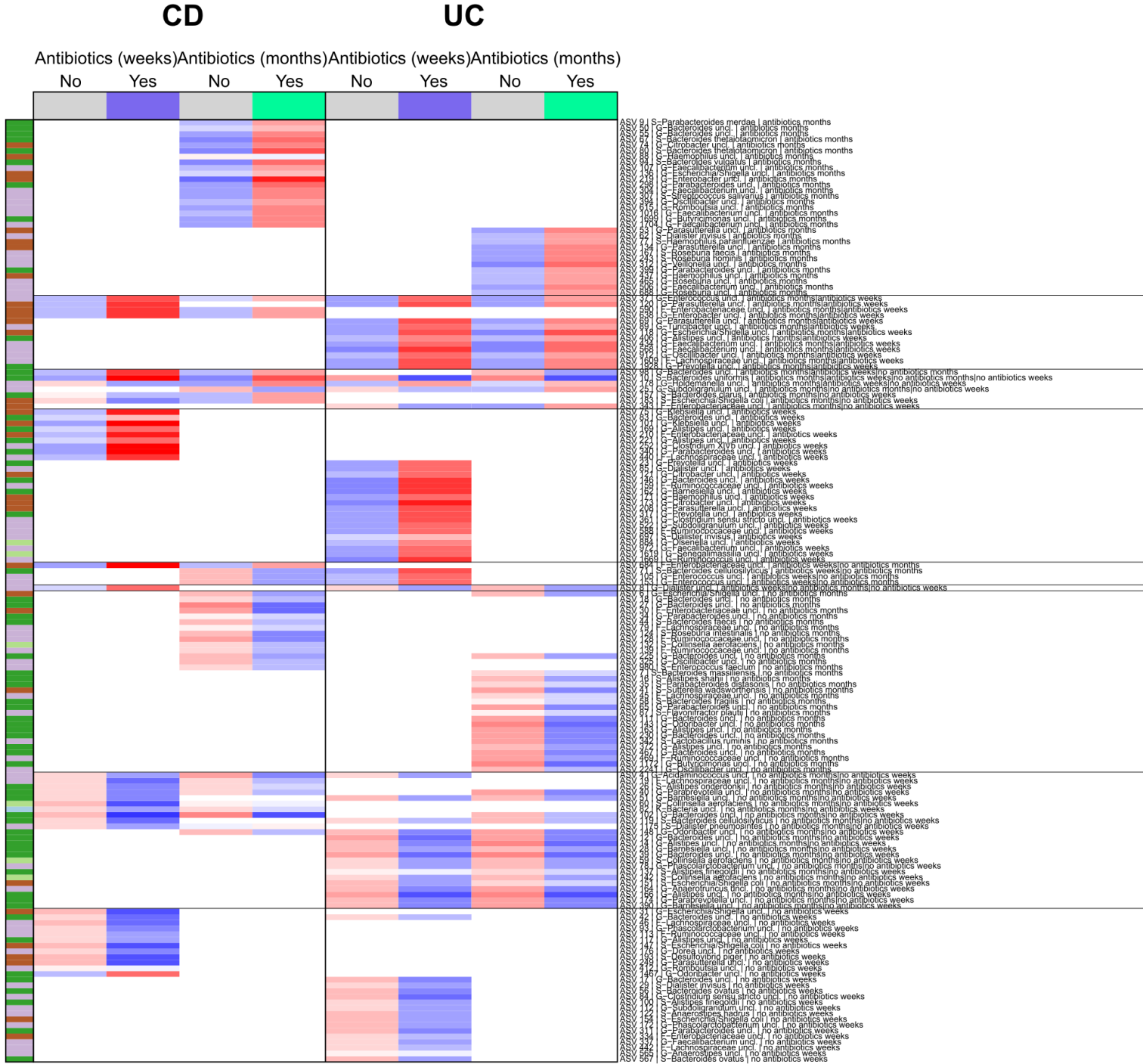


Figure S6: Heatmap visualizing significant differentially abundant ASVs in CD and UC patients with respect to prior antibiotic treatments (Table S5). Differential abundance was tested via DESeq2 and only functions significant after p-value adjustment are displayed.

Crohns disease

Ulcerative colitis

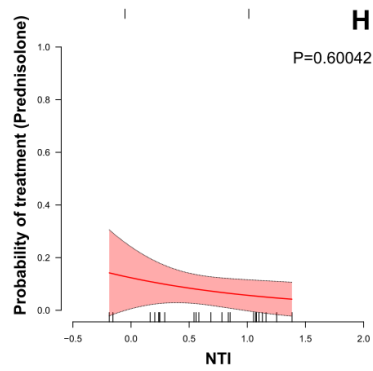
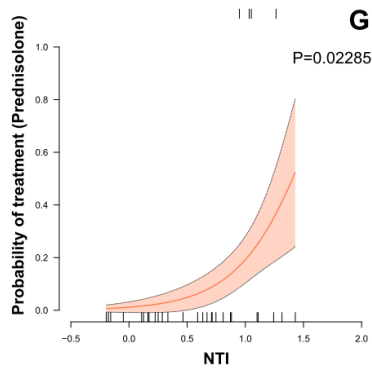
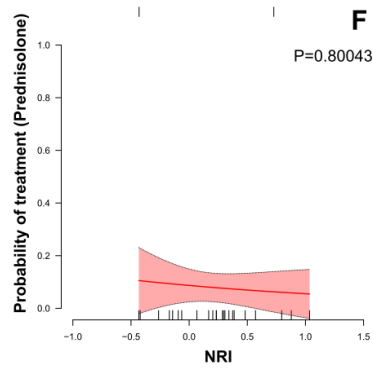
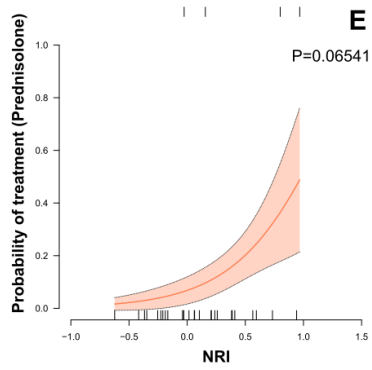
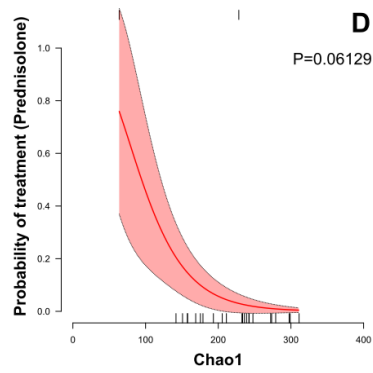
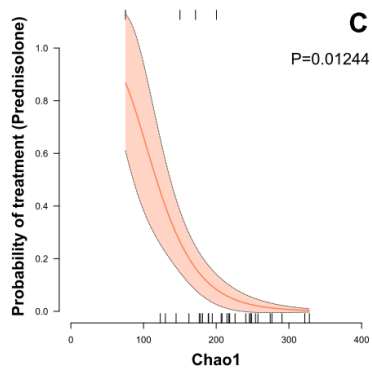
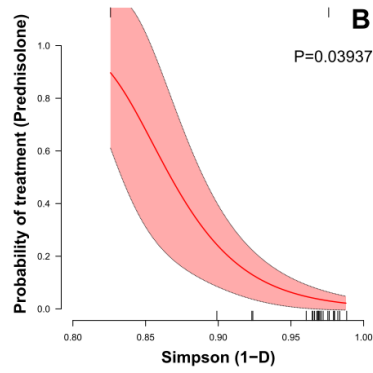
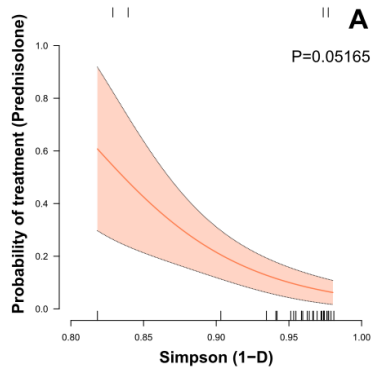


Figure S7: Prediction of treatment probabilities (future treatment with mesalazine, azathioprine, anti-TNF, prednisolone) based on the underlying alpha diversity in CD and UC patients. As single treatment, only corticosteroid treatments are predictable from Simpson diversity (**A:** DF=1,29, Dev.=3.7872, $P=0.05165$, $P_{FDR}=0.24177$; **B:** DF=1,23, Dev.=4.2448, $P=0.03937$, $P_{FDR}=0.61291$), Chao1 species richness (**C:** DF=1,29, Dev.=6.2466, $P=0.01244$, $P_{FDR}=0.20830$; **D:** DF=1,23, Dev.=3.5021, $P=0.06129$, $P_{FDR}=0.61291$), NRI (**E:** DF=1,29, Dev.=3.3945, $P=0.06541$, $P_{FDR}=0.24177$; **F:** DF=1,23, Dev.=0.06391, $P=0.8004$, $P_{FDR}=1.0000$), and NTI (**G:** DF=1,29, Dev.=5.1799, $P=0.02285$, $P_{FDR}=0.20830$; **H:** DF=1,23, Dev.=0.27436, $P=0.6004$, $P_{FDR}=1.0000$). Ticks on the bottom of the graph indicate samples without treatment, ticks on the top indicate samples with future treatment.

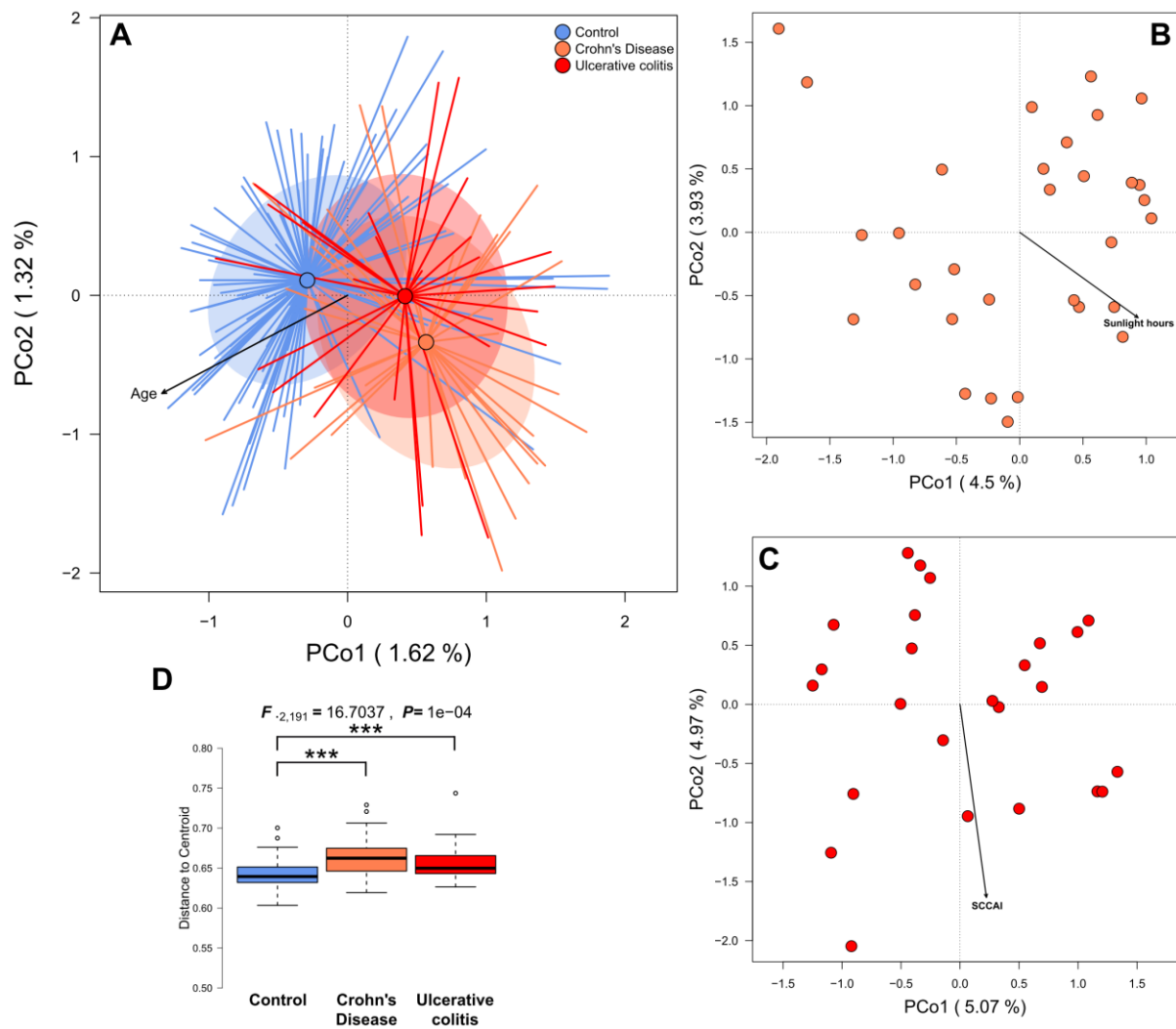


Figure S8: Principle coordinate analyses of Jaccard distance visualizing the differences between the disease cohorts and including nominal significant factors and continuous variables (A), as well as separate betadiversity analyses of only CD- (B) and UC (C) patients. (D) Boxplots visualize the community

variability within each health group measured as distance to the centroid, which is lowest in healthy individuals.

average Z-Value

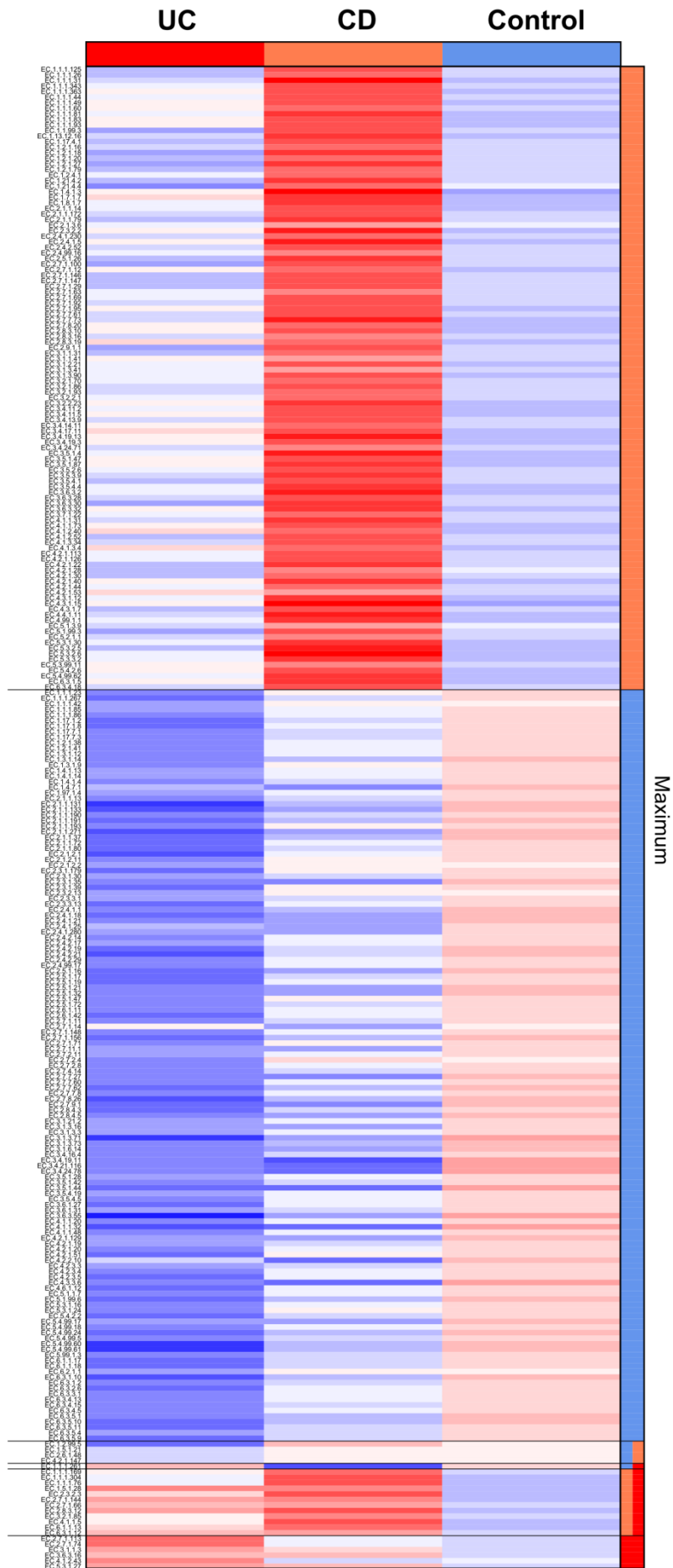
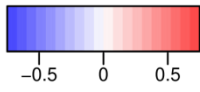


Figure S9: Heatmap visualizing significant differentially abundant functions between healthy controls, CD and UC patients (Table S10). Functions are represented as the PiCRUST2 imputed abundance of single enzymes categories/EC categories (Enzyme Commission number). Differential abundance was tested via DESeq2 and only significantly different functions, after FDR adjustment, are displayed.

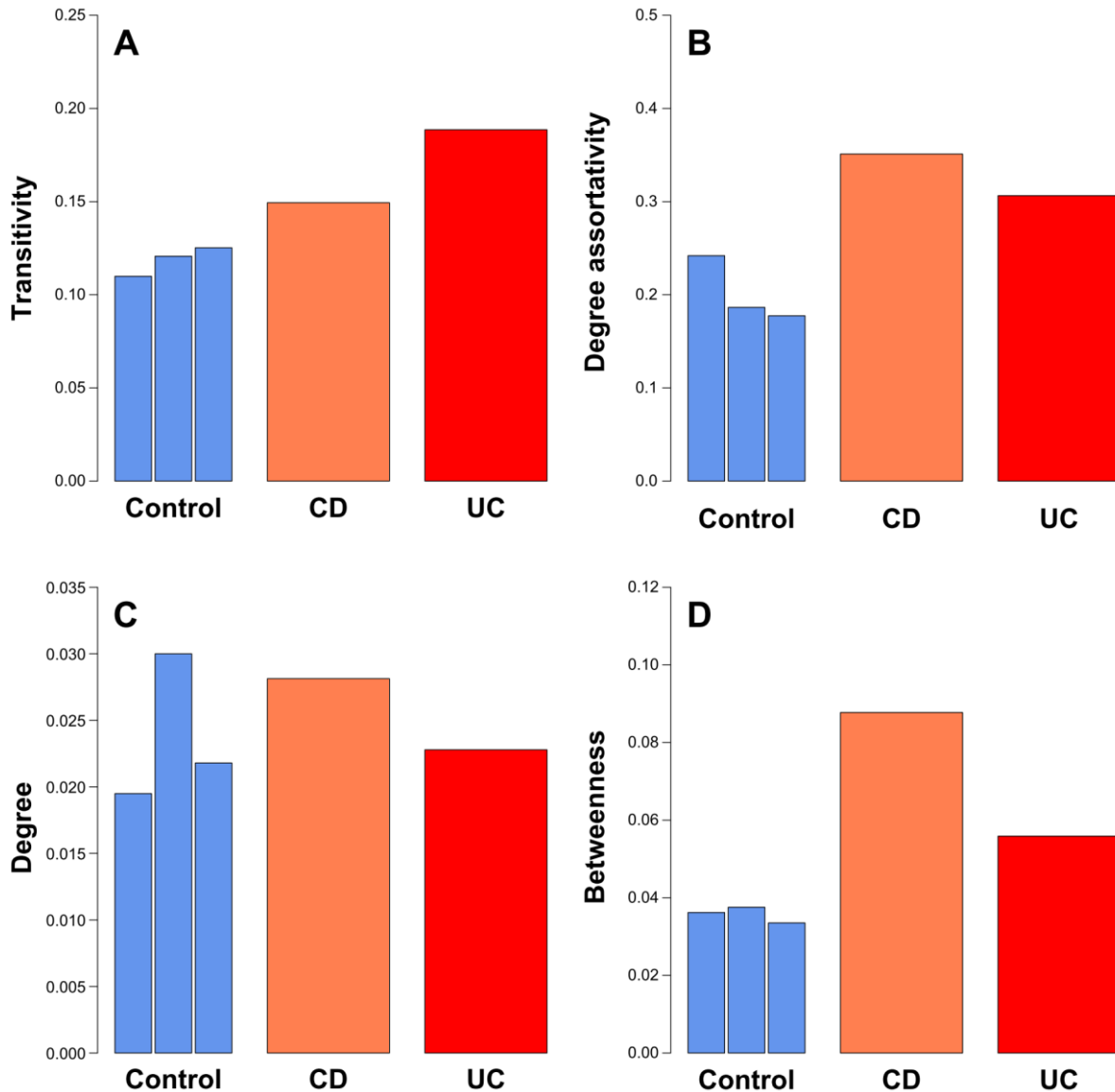
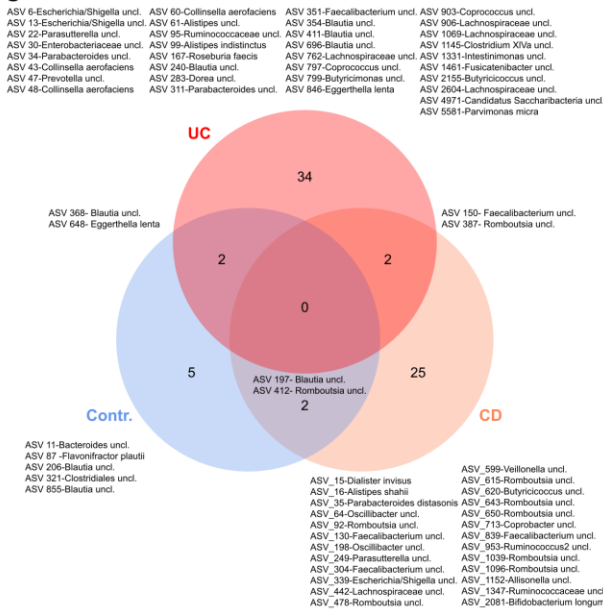


Figure S10: Global network descriptors for each health condition specific network (including subsamples of the control based networks), like **(A)** average transitivity, which describes the clustering and denseness of the respective network. **(B)** Degree assortativity describes preferential attachment of bacteria with similarly connected bacteria, while average degree and betweenness describe the **(C)**

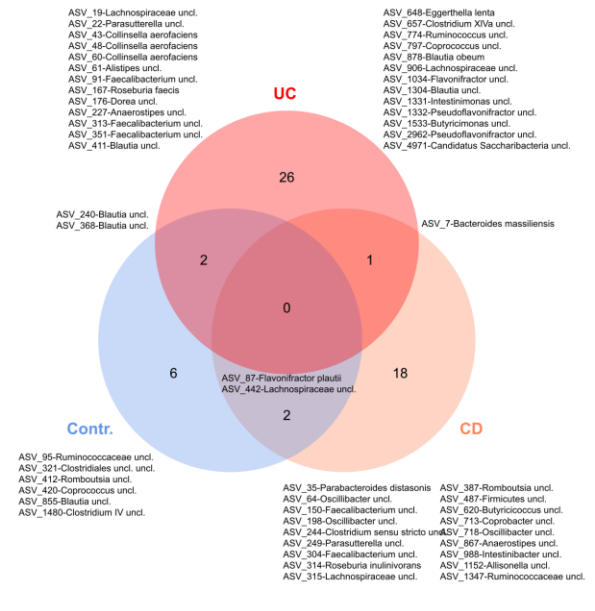
average number of connections of nodes in the network and **(D)** the average of shortest paths in the networks.

Figure S11: Centrality measures of the 50 most important nodes of the respective importance measures (Betweenness, Eigenvalue centrality, PageRank). Red letters highlight network members with a higher importance than expected by chance, based on a Z-test against 10'000 randomized networks ($P \leq 0.05$). Highlighted are the associations of the respective ASVs as detected by differential abundance analysis as well ($P_{FDR} \leq 0.05$, Table S12).

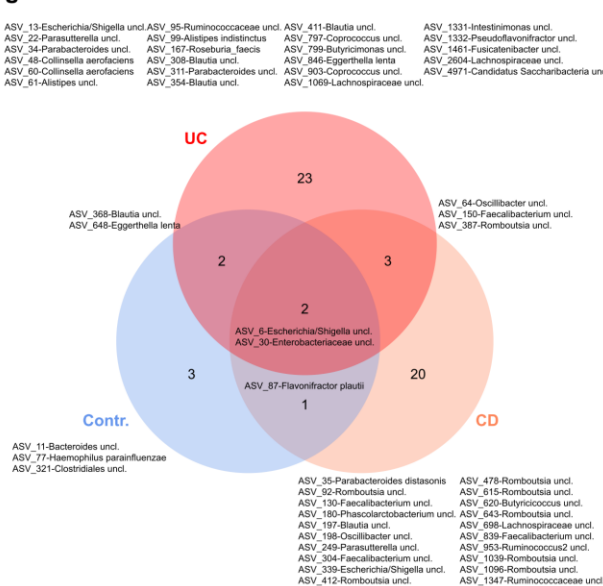
Degree



Betweenness



PageRank



Eigencentrality



Figure S12: Overlapping and private ASVs with significant network positions among health condition specific networks. Centralities in the control cohort were based on the average of three independent

network calculations on three subsamples of the respective cohort to balance differences in cohort sizes (Table S12).

■ sign. important nodes in contr. ■ sign. important nodes in CD
■ sign. important nodes in UC ■ insign. important nodes

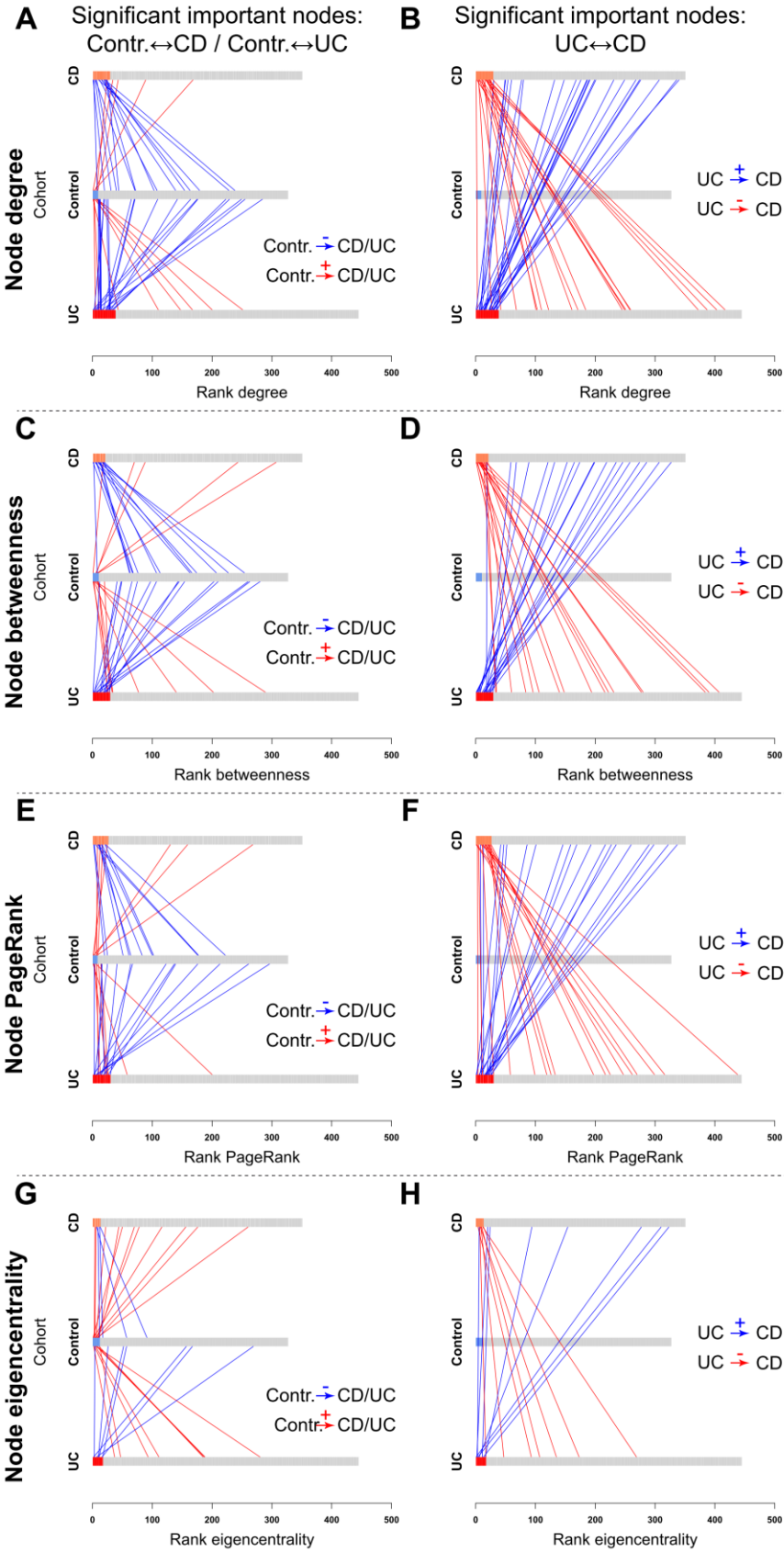


Figure S13: The parallel coordinate plots illustrate the change of positions of significantly central bacteria from one health condition to the other. Single bars visualize nodes ordered by their ranked importance within the respective networks, based on **(A, B)** node degree, **(C, D)** node betweenness, **(E, F)** PageRank index, and eigenvalue centrality **(G, H)**. The first bar shows taxa ranked by their importance in CD specific networks, the second bar taxa ranked by average node importance in networks based on the cohort, and the third bar taxa ranked by their importance in UC specific networks. The change in network position/importance is indicated by lines connecting the same ASVs/nodes between the respective networks/bars. Plots **A, C, E, G** display significant nodes and their respective position/rank in Contr. and CD networks, or Contr., and UC networks. Change of taxa, which increase in importance (smaller rank) when found in a diseased community as compared to the controls is shown in blue, while taxa decreasing in importance (increased rank) in a diseased community are shown in red. Plots **B, D, F, H** display significant nodes and their change in position between CD and UC, with increases of importance (decreasing rank) from CD to UC highlighted in blue, while increases of importance from UC to CD are highlighted in red. Centralities in the control cohort were based on the average of three independent network calculations on three subsamples of the respective cohort to balance differences in cohort sizes.

Supplemental tables

Table S1: Results of differential ASV abundance tests via negative binomial generalized linear models (via *DESeq2*, LR test) with respect to IBD condition and smoking status, corrected for age and BMI. P-values were corrected for multiple testing via FDR-adjustment. ASVs are ordered by the cohort with their maximum abundance and overlaps with significant indicator species are shown. ASVs highlighted in grey are associated with more than one variable.

Table S2: Indicator species analysis abundance analyses of ASVs with respect to IBD- and smoking status ($P \leq 0.05$). ASVs are ordered by their association and overlaps with significant differentially abundant ASVs are highlighted.

Table S3: Differential abundance analyses of ASVs via *DESeq2* (LR test) with respect to IBD subtypes corrected for age and BMI ($P_{\text{FDR}} \leq 0.05$). ASVs are ordered by the cohort with their maximum abundance and overlaps with significant indicator species are shown. Subtypes follow the Montreal classification¹³.

Table S4: Indicator species analysis abundance analyses of ASVs with respect to IBD subtypes ($P \leq 0.05$). ASVs are ordered by their association and overlaps with significant differentially abundant ASVs are highlighted. Subtypes follow the Montreal classification¹³.

Table S5: Differential abundance analyses of ASVs via *DESeq2* (LR test) with respect to medication with non-IBD related medication and prior antibiotic usage (within the last 6 weeks, within the last 6 months) corrected for age and BMI ($P_{\text{FDR}} \leq 0.05$). ASVs are ordered by the cohort with their maximum abundance and overlaps with significant indicator species are shown.

Table S6: Indicator species analysis abundance analyses of ASVs with respect to medication with non-IBD related medication and prior antibiotic usage (within the last 6 weeks, within the last 6 months) ($P \leq 0.05$). ASVs are ordered by their association and overlaps with significant differentially abundant ASVs are highlighted.

Table S7: Analysis of alpha diversity differences in CD and UC patients focusing on non-IBD related pharmaceutical treatments.

Table S8: Betadiversity analysis of CD and UC patients focusing on community variability with respect to anthropogenic and disease related variables, as estimated via a multivariate and permutative version of the Levene's test for homogeneity of variances.

Table S9: Betadiversity analysis of CD and UC patients focusing on anthropogenic and disease related variables (PERMANOVA).

Table S10: Analyses of betadiversity between CD and UC subtypes following the Montreal classification¹³ (PERMANOVA).

Table S11: Differential abundance analyses of predicted functions (EC categories) via *DESeq2* (Wald test) with respect to health condition, corrected for age and BMI ($P_{\text{FDR}} \leq 0.05$). Functions are ordered by the

cohort with their maximum abundance. Each pairwise comparison is shown and only significant differences were evaluated for the direction of change as indicated by their maximum abundance.

Table S12: Differential abundance analyses of predicted pathways (MetaCyc pathways¹⁴) via *DESeq2* (Wald test) with respect to health condition, corrected for age and BMI ($P_{\text{FDR}} \leq 0.05$). Pathways are ordered by the cohort with their maximum abundance. Each pairwise comparison is shown and only significant differences were evaluated for the direction of change as indicated by their maximum abundance.

Table S13: Overview of significantly central ASVs in disease specific ASV correlation networks for healthy controls (average of 3 subsets), CD- and UC patients. The number of connections (degree), their position between different nodes (Betweenness) and their general importance (Eigenvector-centrality and PageRank) were used measures of centrality and their significance was determined by a one-sided Z-Test of the observed values against a null distribution of 10'000 permuted networks. Associations to different anthropometric characteristics, as detected via indicators species analyses ($P \leq 0.05$) and differential abundance analyses ($P_{\text{FDR}} \leq 0.05$), are included in the table. The color-code highlights in which networks ASVs are repeatedly important (■-important across all health conditions, ■-important only in control networks, ■-important only in the CD network, ■-important only in the UC network).

Supplemental references

- 1 Caporaso JG, Lauber CL, Walters WA, et al. Ultra-high-throughput microbial community analysis on the Illumina HiSeq and MiSeq platforms. *ISME J.* 2012.
- 2 Callahan BJ, McMurdie PJ, Rosen MJ, Han AW, Johnson AJA, Holmes SP. DADA2: High-resolution sample inference from Illumina amplicon data. *Nat Meth.* Brief Communication. 2016;13(7):581-583.
- 3 Wang Q, Garrity GM, Tiedje JM, Cole JR. Naive Bayesian Classifier for Rapid Assignment of rRNA Sequences into the New Bacterial Taxonomy. *Applied and environmental microbiology.* Research Support, U.S. Gov't, Non-P.H.S. 2007;73(16):5261-5267.
- 4 Cole JR, Wang Q, Cardenas E, et al. The Ribosomal Database Project: improved alignments and new tools for rRNA analysis. *Nucl Acids Res.* 2009;37(suppl_1):D141-145.
- 5 Schloss PD. A High-Throughput DNA Sequence Aligner for Microbial Ecology Studies. *PLoS One.* 2009;4(12).
- 6 Schloss PD, Westcott SL, Ryabin T, et al. Introducing mothur: Open Source, Platform-independent, Community-supported Software for Describing and Comparing Microbial Communities. *Applied and environmental microbiology.* Research Support, Non-U.S. Gov't. 2009;75(23):7537-7541.
- 7 Pruesse E, Quast C, Knittel K, et al. SILVA: a comprehensive online resource for quality checked and aligned ribosomal RNA sequence data compatible with ARB. *Nucl Acids Res.* 2007;35(21):7188-7196.
- 8 Quast C, Pruesse E, Yilmaz P, et al. The SILVA ribosomal RNA gene database project: improved data processing and web-based tools. *Nucleic Acids Res.* 2013;41(Database issue):D590-596.
- 9 Price MN, Dehal PS, Arkin AP. FastTree 2 – Approximately Maximum-Likelihood Trees for Large Alignments. *PLoS One.* Research Support, U.S. Gov't, Non-P.H.S. 2010;5(3):e9490.
- 10 Gotelli NJ. Null model analysis of species co-occurrence patterns. *Ecology.* 2000;81(9):2606-2621.
- 11 Kembel SW, Cowan PD, Helmus MR, et al. Picante: R tools for integrating phylogenies and ecology. *Bioinformatics.* Research Support, Non-U.S. Gov't
Research Support, U.S. Gov't, Non-P.H.S. 2010;26(11):1463-1464.
- 12 Friedman J, Alm EJ. Inferring Correlation Networks from Genomic Survey Data. *PLoS Computational Biology.* 2012;8(9):e1002687.
- 13 Satsangi J, Silverberg MS, Vermeire S, Colombel JF. The Montreal classification of inflammatory bowel disease: controversies, consensus, and implications. *Gut.* 2006;55(6):749-753.
- 14 Karp PD, Riley M, Paley SM, Pellegrini-Toole A. The MetaCyc Database. *Nucleic Acids Res.* 2002;30(1):59-61.